An Evaluation of the practicability of current mapping functions using ray-traced delays from JMA Mesoscale Numerical Weather Data

Ryuichi Ichikawa, Thomas Hobiger, Yasuhiro Koyama
Space-time standards group, Kashima Space Research Center,
National Institute of Information and Communications Technology (NICT), Japan

Tetsuro Kondo
National Institute of Information and Communications Technology (NICT), Japan
Department of Space Survey and Information Technology, Ajou University, Republic of Korea

Contact: richi@nict.go.jp

BIOGRAPHY

Ryuichi Ichikawa received his M.Sc. and Ph.D. degrees in geodesy and geophysics from Hokkaido University, Sapporo, Japan in 1990 and 1994, respectively. He joined the VLBI research group of the Kashima Space Research Center, Communications Research Laboratory (CRL) in 1995. His research interests include the development of a compact VLBI system for geodesy, studies of tropospheric refraction, GNSS, VLBI and physics of the solid Earth.

Thomas Hobiger received his M.Sc. and Ph.D. degrees in geodesy and geophysics from the Vienna University of Technology, Austria in 2002 and 2005, respectively. From October 2006 until September 2008 he worked at Kashima Space Research Center, National Institute of Information and Communications Technology (NICT), Japan as a JSPS fellow. His research interests include troposphere and ionosphere modeling, GNSS, Very Long Baseline Interferometry (VLBI), adjustment theory and high performance computing.

Yasuhiro Koyama received the Ph.D. degree in Astronomy from the Graduate University for Advances Studies, Japan in 2003. He has been involved in the research and development of VLBI since he joined the research group of the Radio Research Laboratory (now National Institute of Information and Communications Technology) in 1988.

Tetsuro Kondo received the Ph.D. degree in geophysics from Tohoku University, Sendai, Japan, in 1982. He joined the staff of the Kashima Space Research Center, Communications Research Laboratory (CRL) in 1981 and worked on the development of VLBI technology and analysis of space geodetic techniques. Since April 2008, he is research professor at Ajou University, Korea.

ABSTRACT

The the Japan Meteorological Agency (JMA) meso-scale analysis data (MANAL data) which we used in our study provides temperature, humidity, and pressure values at the surface and at 21 height levels (which vary between several tens of meters and about 31 km), for each node in a 10km by 10 km grid that covers Japan islands, the surrounding ocean and eastern Eurasia. The 3-hourly operational products are available by JMA since March, 2006. We have simultaneously evaluated atmospheric parameters (equivalent zenith total delay and linear horizontal delay gradients) and position errors derived from slant path delays obtained by the KAshima RAytracing Tools (KARAT) through the MANAL data. Most of the early mapping functions developed for VLBI and GPS were based on the assumption of azimuthal isotropy. On the other hand, the recent geodetic analyses are carried out by applying the modern mapping functions based on the numerical weather analysis fields. The Global Mapping Function (GMF) by Boehm et al. (2006), and Vienna Mapping Function (VMF) by Boehm and Schuh (2004) have been successfully applied to remove the zenith hydrostatic delay in the recent years. In addition, the lateral spatial variation of wet delay is reduced by linear gradient estimation. Comparisons between KARAT-based slant delay and empirical mapping functions indicate large biases ranging from 18 to 90 mm, which is considered to be caused by significant variability of water vapor. Position error simulation reveal that the highly variability of the errors is clearly associated with severe atmospheric phenomena. Such

simulation are very useful to investigate the characteristics of positioning errors generated by local atmospheric disturbances. Finally, we compared PPP processed position solutions using KARAT with those using the latest mapping functions covering a period of two week GEONET data. The KARAT solution is almost identical to the solution using GMF with linear gradient model, but some cases tends to be slightly worse under the extreme atmospheric condition. Though we need further investigations to evaluate the capability of KARAT to reduce atmospheric path delay under the various topographic and meteorological regimes, KARAT will promise an efficient reduction of atmospheric path delays considering that the numerical weather model will be improved concerning spatial and temporal resolution

INTRODUCTION

Radio signal delay associated with the neutral atmosphere is one of the major error sources in GNSS, VLBI, In-SAR measurements. Recently, several anisotropic mapping functions have been developed for the purpose of a better modeling of these propagation delays, thereby improving the repeatability of horizontal site coordinates (MacMillan, 1995; Chen and Herring, 1997). The anisotropic mapping function is a powerful tool for removing or calibrating the effects of horizontal variability of atmosphere within GNSS and VLBI analyses. Atmospheric gradients are assumed to have a simple linear form modeled by the anisotropic mapping function. However, it has been suggested that this assumption is not always appropriate in the context of intense mesoscale phenomena such as the passing of a cold front, heavy rainfall, or severe storms.

We have developed a new tool to obtain atmospheric slant path delays by ray-tracing through the meso-scale analysis data from numerical weather prediction with 10 km horizontal resolution provided by the Japan Meteorological Agency (JMA) (Hobiger et al., 2008a) (hereafter, we call this "JMA 10km MANAL data"). These data are operationally used weather forecast and are considered for our study. We have created ray-tracing routines and named the tools "KAshima RAytracing Tools (KARAT)" resolution (Hobiger et al., 2008a). First, we compared empirical mapping functions, developed space geodesy, with KARAT slant delays. Next, we estimated position changes caused by the horizontal variability of the atmosphere by running simulations using the ray-traced slant delays in order to examine the position error magnitude and its behavior under meso-scale atmospheric disturbances. Finally, we carried out a preliminary comparison between position repeatabilities of precise point positioning (PPP) estimates using KARAT and those using the latest mapping function.

ATMOSPHERIC PATH DELAY

The refractivity, N, and the refractive index, n, of the neutral atmosphere are well described by the equation (Bevis et al., 1994)

$$N = (n-1) \times 10^6 = 77.6 \times \left(\frac{P}{T}\right) + 3.82 \times 10^5 \left(\frac{P_v}{T^2}\right) \quad (1)$$

where P is total pressure, P_v is the partial pressure of water vapor, and T is temperature. The first and second terms on the right hand side of equation (1) are referred to as the hydrostatic and wet components of refractivity, respectively. Because water vapor is largely confined to the lower troposphere, the scale height associated with the wet delay is considerably smaller than that of the hydrostatic delay.

The usual geodetic approach of calibrating the neutral delay is to model the delay at each station (for a certain period of time) in terms of one or more parameters, and to jointly estimate the time development of these parameters for the entire network. The simplest approach is to ignore the azimuthal anisotropy of the neutral atmosphere, and assume that the delay at an arbitrary elevation ε can be represented as the product of the zenith delay (i.e. the delay for a vertical raypath) and a mapping function, $m(\varepsilon)$, that describes the elevation dependence (e.g. Niell [1996, 2001], Boehm et al. [2004, 2006a, 2006b]). Thus the neutral delay associated with a given station is specified by the time development of its zenith delay parameter, which might be treated as piecewise constant, piecewise linear, or as a stochastic process. The isotropic model for the atmospheric delay $\Delta L(\varepsilon)$ (*ZTD*: zenith total delay) for a path with elevation angle ε is

$$\Delta L(\varepsilon) = \Delta L_h^z M_h(\varepsilon) + \Delta L_w^z M_w(\varepsilon) \quad (2)$$

where ΔL^Z_h is the zenith hydrostatic delay, $M_h(\varepsilon)$ is the hydrostatic mapping function, ΔL^Z_w is the zenith wet delay, and $M_w(\varepsilon)$ is the wet mapping function. Both $M_h(\varepsilon)$ and $M_w(\varepsilon)$ are isotropic mapping functions depending only on the elevation angle of the raypath.

Accordingly, geodesists are turning to generalized mapping functions that incorporate azimuthal anisotropy (MacMillan, [1995]; Chen and Herring, [1997]) and routinely estimating gradient parameters as well as zenith delay parameters (e.g. BarSever and Kroger, [1998]). For example, Chen and Herring [1997] introduced an anisotropic model for atmospheric delay with the following form

$$\begin{aligned} \Delta L \;=\; & \Delta L_h^z M_h(\varepsilon) + \Delta L_w^z M_w(\varepsilon) \\ & + L_{ns} m_{az}(\varepsilon)\cos\alpha + L_{ew} m_{az}(\varepsilon)\sin\alpha \end{aligned} \quad (3)$$

where L_{ns} and L_{ew} are north-south and east-west gradient parameters, $m_{az}(\varepsilon)\cos\alpha$ and $m_{az}(\varepsilon)\sin\alpha$ are the gradient mapping functions, and

$$m_{az}(\varepsilon) = 1/(\sin\varepsilon\tan\varepsilon + C) \quad (4)$$

where C is a constant. The first two terms in equation (3) correspond to the isotropic model, and the second pair of terms parameterizes the purely anisotropic delay. Note that the form of these new terms ensures that at a fixed elevation angle the anisotropic delay has a mean value of zero over the full range of azimuths, and at a fixed azimuth the anisotropic component of delay declines with increasing elevation angle until it vanishes at zenith (ε = 90°). It is important to realize that the gradient terms in equation (3) are normally used to model anisotropy derived from both the hydrostatic and the wet refractivity structure of the atmosphere. In this case the optimum value of C is close to 0.0032 (Chen and Herring, 1997).

KARAT

KARAT have been developed at the National Institute of Information and Communications Technology (NICT), Japan and is capable of calculating total slant delays and ray-bending angles. We perform a successive 19 months run of KARAT calculations from March 2006 to September 2007. The JMA 10km MANAL data which we used in our study provides temperature, humidity, and pressure values at the surface and at 21 pressure levels (which are equal to steps of several meters to kilometers up to about 31 km), for each node in a 10 km by 10 km grid that covers all Japanese islands, the surrounding ocean and Eastern Asia (Saito et al., 2006). Figure 1 shows the distribution of the total zenith delays retrieved from the JMA 10-km MANAL data at 1600 UT of July 22nd, 2006.

We first resample the original JMA grid to a modified grid which allows to run the new ray tracing algorithms using analytic expressions. At present the 3-hourly operational products are only available by JMA. Thus, a linear time interpolation is used to obtain results at arbitrary epochs what allows also to evaluate temporal change of estimates. The details of KARAT is described in another paper (Hobiger et al., 2008a).

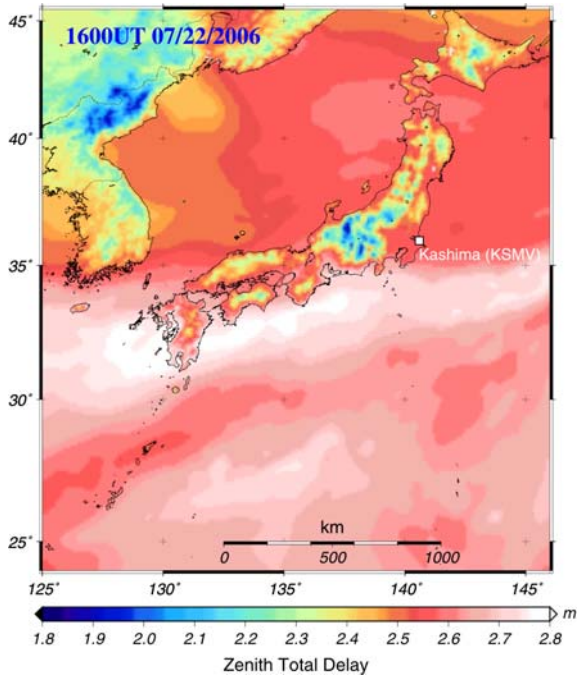

Figure 1: Zenith total delay retrieved by the JMA 10km MANAL data at the 1600UT of July 22, 2006.

COMPARISON BETWEEN MAPPING FUNCTIONS AND KARAT-BASED SLANT DELAY

We compare empirical mapping functions developed for GPS and VLBI with equivalent slant delays estimated by KARAT. Modern mapping functions such as the Isobaric Mapping Function (IMF) (Niell, 2001), Global Mapping Function (GMF) (Boehm et al., 2006a), and Vienna Mapping Function (VMF) (Boehm and Schuh, 2004) have been successfully used to estimate site dependent zenith delays in the past few years. The lateral spatial variation of wet delay is reduced by linear gradient estimation. However, the mapping function errors associated with the lateral heterogeneity of the atmosphere have not been assessed sufficiently so far. Our aim is to see how well the modern anisotropic mapping functions can mimic the directional variability associated with the intense mesoscale disturbances typical of the Japanese monsoon.

Figure 2 shows the three typical mapping functions (NMF, VMF, GMF) for station Kashima (a location is shown in Figure 1), Japan from 2005 to the middle of 2008. The Niell Mapping Function (NMF) (Niell, 1996) is still widely used by many geodesists. Because it depends only on the station latitude, height and the day of the year, users can easily apply it within data processing without in-situ meteorological measurements. However, NMF has significant scale biases reaching values up to 0.015 at an elevation of 5° in winter-spring season in eastern Asia region as compared to VMF and GMF, shown in Figure 2. Such biases can lead to significant station height errors.

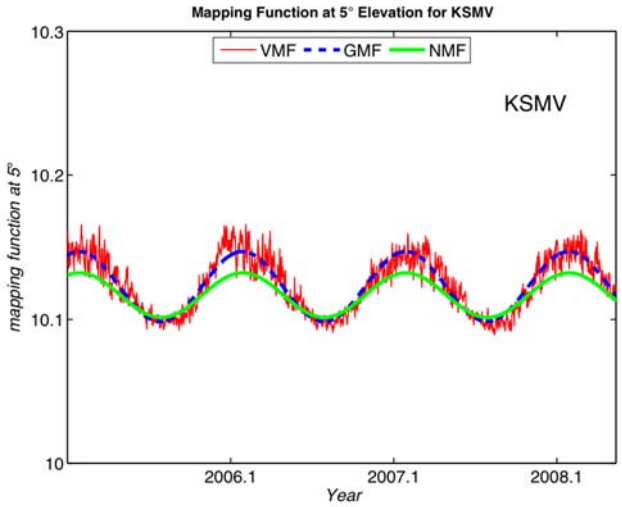

Figure 2: Mapping functions VMF (red, thin solid), GMF (blue, dash-dot), and NMF (green, solid) for 5° elevation at Kashima, Japan (IGS station: KSMV), from 2005 to the middle of 2008.

On the other hand, both GMF and VMF are considered to be globally available to reduce atmospheric path delays for GNSS and VLBI processing. In order to assess the availability of these mapping functions in the East Asia region, we compared KARAT-based slant delays at elevation of 5° with each mapping function values at 16 IGS stations. We examined both the mean and standard deviation of slant delay residuals. The mean value represents a bias associated with each mapping function, whereas the standard deviation value represents the scatter due to horizontal variability of atmosphere (mainly caused by water vapor variation). The results are summarized in Table 1 and one example histogram of the residuals at Kashima is shown in Figure 3.

Table 1: Mean bias and standard deviation values in millimeter of slant delay residuals at elevation of 5° for 16 IGS stations in the East Asia region.

IGS	VMF-KARAT	GMF-KARAT	NMF-KARAT
YSSK	-8.3±18.7	-10.8±30.6	-14.1±32.3
MIZU	16.1±43.6	21.9±50.1	31.3±51.0
TSKB	12.3±48.8	22.6±52.7	38.4±53.4
KSMV	8.9±45.0	19.0±49.6	34.7±50.2
KGNI	20.7±44.9	27.3±49.7	43.7±50.1
MTKA	17.9±44.1	25.4±48.4	41.9±48.8
USUD	56.9±32.1	1.6±35.1	12.1±35.5
BJFS	13.6±37.7	14.6±42.4	24.8±42.9
DAEJ	16.4±64.6	18.9±68.7	36.5±69.7
SUWN	-0.6±54.0	4.0±59.4	20.0±59.3
AIRA	-78.5±65.4	-93.9±63.1	-82.1±63.0
GMSD	6.5±50.2	0.5±53.4	25.2±54.9
CCJM	15.8±65.0	2.5±66.0	28.4±66.7
TWTF	21.5±79.7	5.3±80.0	42.5±81.4
TCMS	63.5±93.3	53.8±92.9	92.9±94.1
TNML	63.5±93.3	53.9±92.9	93.0±94.1

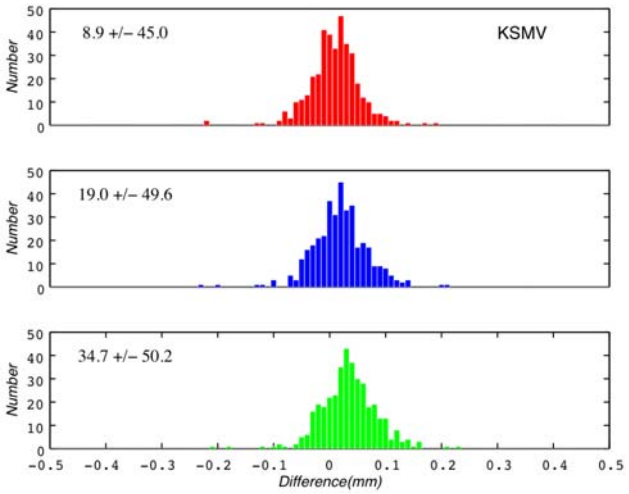

Figure 3: Histogram of residuals in slant delays at elevation of 5° from the end of June to September, 2007. Values between VMF and KARAT (upper), those between GMF and KARAT (middle), and those between NMF and KARAT (lower) are shown, respectively.

Numerical weather model data are based on the physical/dynamical equations that govern the atmospheric flow. The JMA 10 km MANAL data are obtained by combining short model forecasts with new observations (a process called data assimilation). Therefore, the ZTD obtained from KARAT can be considered to be the most realistic empirical value of the real atmosphere.

Large biases of more than 10 mm occur at almost stations, even if VMF is applied. In addition, the scatter of the residuals for all mapping functions is extremely large ranging from 18 to 90 mm, which is caused by significant variability of water vapor. Though these results suggest that the latest mapping functions are insufficient to remove atmospheric path delay in the East Asia region, we need further investigations to understand the behavior of the atmospheric parameters under the various topographic and meteorological regimes.

SIMULATED POSITION ERROR

For each virtual receiver location we invert the simulated slant delays using an isotropic and an anisotropic delay model. The isotropic model has only one parameter - the zenith total delay (ZTD). The anisotropic delay model (e.g. Chen and Herring, [1997]) has two additional lateral gradient parameters. We compare the 'true' ZTD, computed by directly integrating the atmospheric refractivity field of the grid data, with the ZTD estimated by least squares inversion of the 'observed' slant delays obtained by ray tracing. We did this using the isotropic and the anisotropic delay model.

In addition we estimate atmospheric parameters numerically, and evaluate site position changes from the ray-traced slant delays, assuming single point positioning

without coordinate constraints. We consider the vector between the true position and estimated position to be the positioning error. This estimation is performed to investigate the behavior of the positioning errors generated by local atmospheric disturbances, as well as the relation between the slant delay errors and the vertical positioning errors. Our calculation scheme is illustrated in the Figure 4.

A general expression of a linearized observation equation is described by the equation

$$\boldsymbol{Y} = \boldsymbol{AD} + \boldsymbol{e} \quad (5)$$

where column vector $\boldsymbol{Y}$ contains the results of experimental measurement. The matrix $\boldsymbol{A}$ is called the design matrix which is based on a linear model for the system. Column vector $\boldsymbol{D}$ contains the unknowns of the model and column vector $\boldsymbol{e}$ represents measurement errors.

In our numerical simulation, the column vector $\boldsymbol{D}$ contains a apparent position displacements *(dx, dy, dz)*, atmospheric zenith delay ΔL^Z, and clock offsets of receiver. The $\boldsymbol{Y}$ contains calculated slant delays for each epoch and each line of sight. Here, we assume the column vector $\boldsymbol{e}$ equals $\boldsymbol{0}$. The design matrix $\boldsymbol{A}$ is given by

$$\boldsymbol{A} = [-\cos\varepsilon\cos\phi, -\cos\varepsilon\sin\phi, -\sin\varepsilon, m(\varepsilon), 1] \quad (6)$$

where $m(\varepsilon)$ is the mapping function. $\boldsymbol{D}$ can be obtained by

$$\boldsymbol{D} = (\boldsymbol{A}^T\boldsymbol{A})^{-1}\boldsymbol{A}^T\boldsymbol{Y} \quad (7)$$

When the atmospheric gradient vector is also estimated equation (6) changes to

$$\boldsymbol{A} = [-\cos\varepsilon\cos\phi, -\cos\varepsilon\sin\phi, -\sin\varepsilon, m(\varepsilon), \cos\phi, \sin\phi, 1] \quad (8)$$

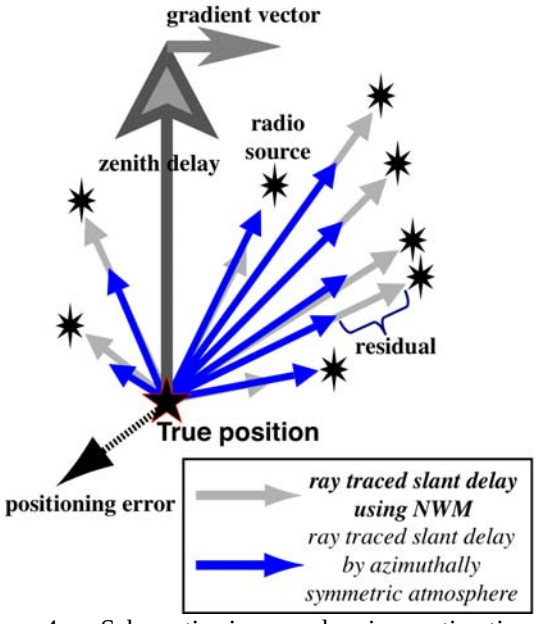

Figure 4: Schematic image showing estimations of atmospheric parameters and position error.

It is also possible to obtain snapshot images of varying positioning errors using the JMA 10km MANAL data field every three hours. These are quite useful for the provision of animated ZTD fields and position estimation errors (Figures are not shown.). E.g., in the western region of Japan, heavy rainfall events occurred during July 18-24, 2006. The hourly rain gauge data over southern Kyushu island recorded more than 50 mm. In addition, total rainfall around Kagoshima area exceeded 1000 mm during 10 days.

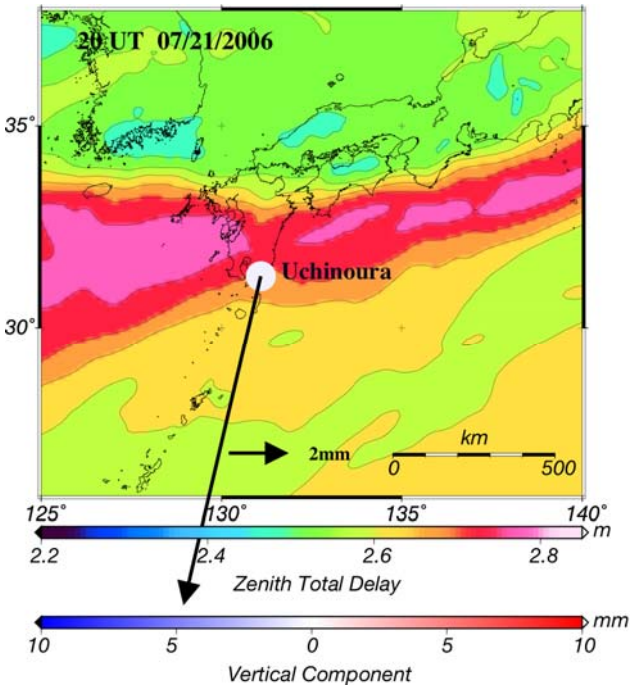

Figure 5: Zenith total delay field and simulated position error at Uchinoura retrieved by the JMA 10km MANAL data at the 2000UT of July 21, 2006.

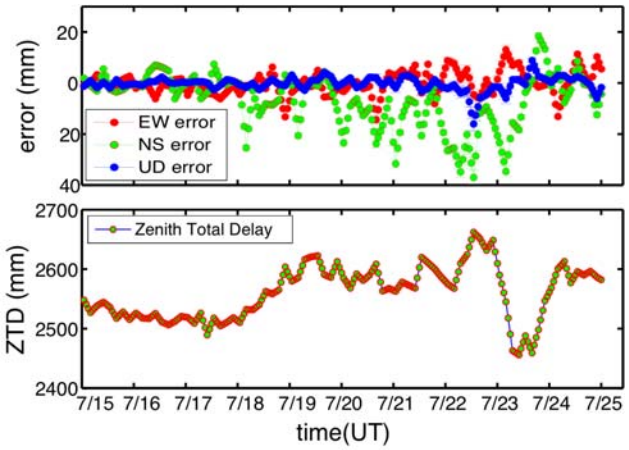

Figure 6: Time series plot of simulated position error (upper) and zenith total delay (lower) at Uchinoura from 14 to 24 July 2006.

Figure 5 shows an example of such images showing the estimated error obtained at Uchinoura GPS station, which is located south of Kyushu island, Japan, at 20:00UT of July 21, 2006. We were able to simulate the large horizontal positioning error which go along with such severe weather conditions. The error vector shown in the figure points SSW and its magnitude is up to 2 cm. This error is caused by steep water vapor gradient associated with a EW rain band which lies north of Uchinoura. The rain band location coincides with a high ZTD band shown in Figure 5. Highly variable position errors associated with same phenomena are also presented after July 19, 2006 (see Figure 6). Especially, a remarkable drop of ZTD and north error component up to 10-40 mm within 10 hours on July 23 is due to a northward moving of the rain band.

PRECISE POINT POSITIONING RESULTS FOR GEONET STATIONS

In order to compare KARAT processing and empirical mapping functions we analyzed whole data sets of GEONET (GPS Earth Observation Network System), which is a nationwide GPS network operated by Geographical Survey Institute (GSI). In our comparison about 1360 stations of GEONET data during July 9th – 23rd of 2007 were processed.

At first, precise point positioning (PPP) estimates covering the whole period shown above were obtained for all sites using GPSTOOLS (Takasu and Kasai, 2005). The troposphere delays have been modeled by dry (using the Saastamoinen [1972] model) and wet constituents, whereas the latter one were estimated as unknown parameters using the GMF together with linear gradients. The daily position estimates from this solution acts a reference to which the ray-traced solutions can be compared (see Hobiger et al., [2008c] in detail.). In our comparison, PPP estimations using the GMF without linear gradient were also performed.

Changes in the mapping functions primarily cause changes of the station heights in general. According to Hobiger et al. (2008a), the KARAT solutions are better than the solutions using GMF with gradient during a period of 4 months. In our comparison, the averaged vertical repeatabilities of all solutions demonstrate a similar nation-wide pattern as shown in Figure 7. The largest repetabilities more than 10 mm, which occur in Kyushu and Shikoku islands which are located in the west of Japan, are reflected in all three figures. In addition, Figure 8, which shows the repetabilities for each coordinate component (i.e. the north, east, and vertical errors) for all three solutions, indicates that the KARAT solution is slightly worse than the GMF with gradient solution. On the other hand, KARAT solution is better than the GMF without gradient solution for horizontal component.

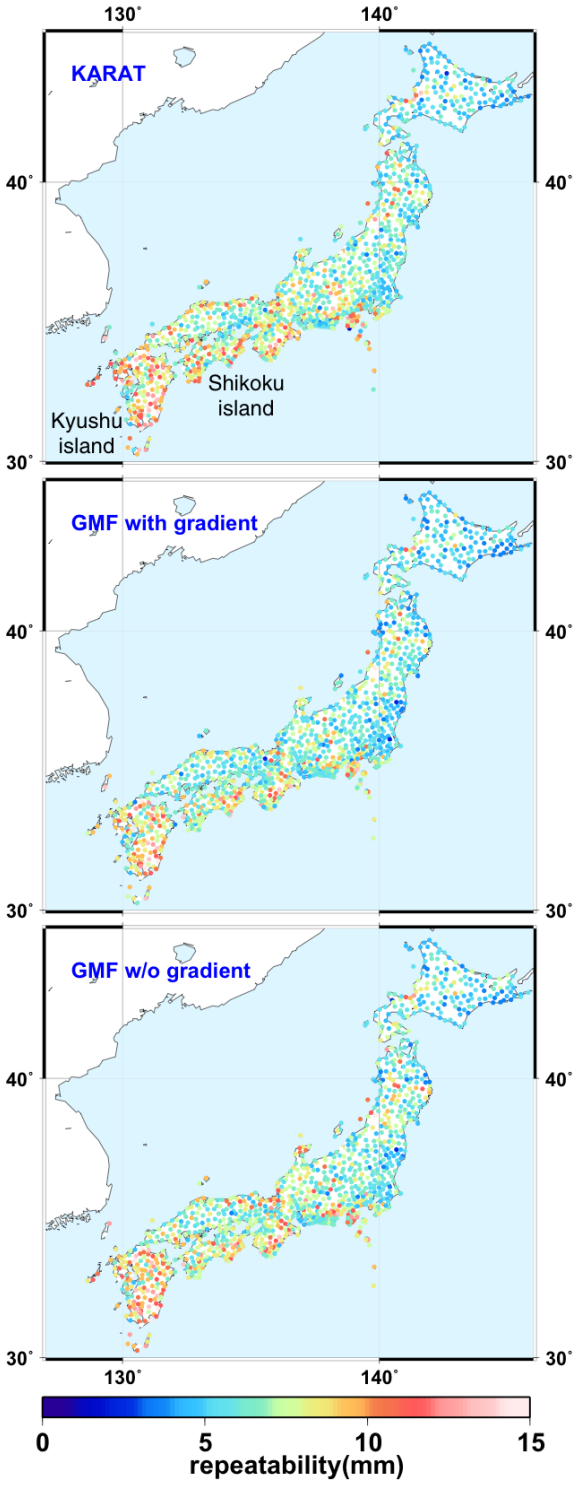

Figure 7: Averaged repetabilities of station height components between July 9th – 23rd of 2007 for all GEONET stations. The upper represents the solution using KARAT, the middle represents the solution using GMF with gradient, and the lower represents the solution using GMF without gradient.

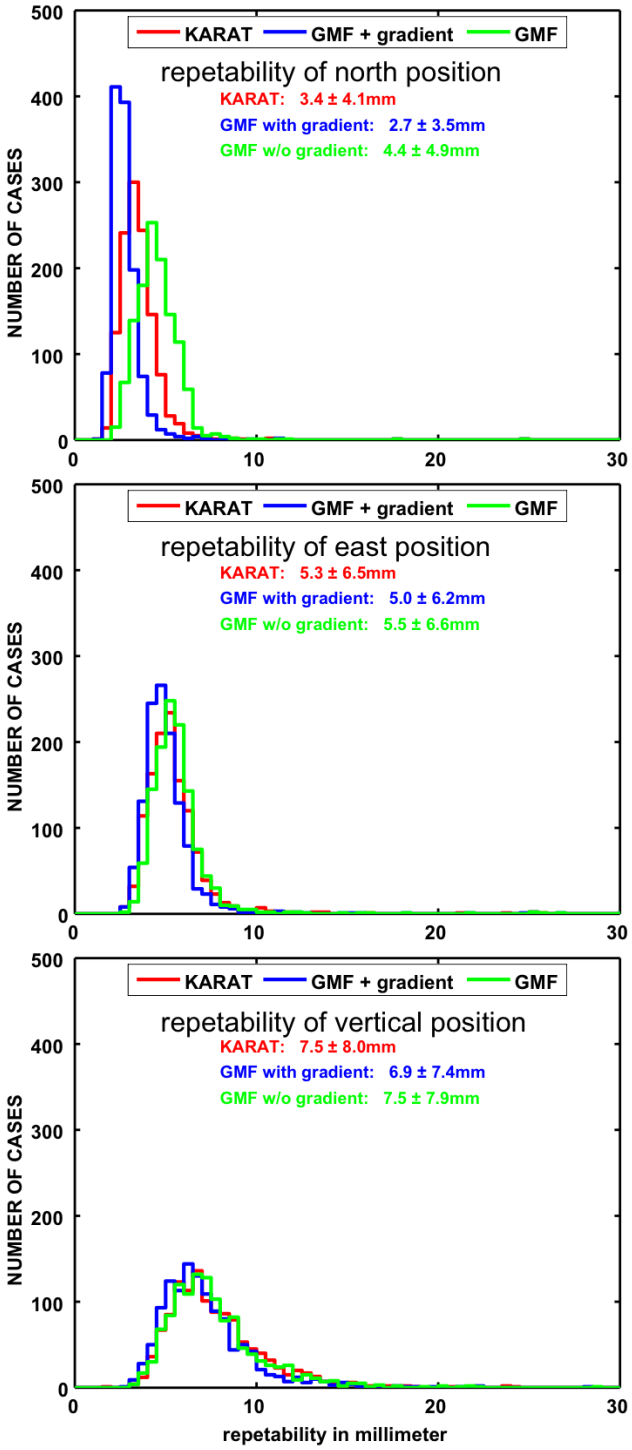

Figure 8: Histogram of repeatabilities for each coordinate component (north, east, and vertical) for each solution.

During the whole processed period both Kyushu and Shikoku islands have undergone severe heavy rain fall event due to the Baiu front and the tyhoon "MAN-YI" passing and cumulating in precipitation amounts ranging 500 - 1100 mm. The time-resolution of the JMA 10km MANAL data is three hours, whereas the PPP processing including gradient estimation was performed for 300 seconds interval. Under the extreme atmospheric condition such as the concerned period, out results imply that the performance of KARAT is almost equal to the solution using the GMF with gradient. We need to extend the processing period for our comparison in order to evaluate a KARAT capability in a reduction of atmospheric path delay.

The advantage of KARAT is an efficient reduction of atmospheric path delay with the numerical weather model improvement (i.e. time and spatial resolution, including new observation data). In spite of the present model imperfectness and coarse time resolution, we hope KARAT will liberate station position determination from numerical instability of unknown parameters.

SUMMARY

We have simultaneously evaluated atmospheric parameters (equivalent zenith total delay and linear horizontal delay gradients) and position errors derived from slant path delays obtained by the KAshima RAytracing Tools (KARAT) through the Japan Meteorological Agency 10 km meso-scale analysis data (JMA 10 km MANAL data). The JMA 10 km MANAL data which we used in our study provides temperature, humidity, and pressure values at the surface and at 21 height levels (which vary between several tens of meters and about 31 km), for each node in a 10km by 10 km grid that covers Japan islands, the surrounding ocean and eastern Eurasia. The 3-hourly operational products are available by JMA since March of 2006.

The comparisons between KARAT-based slant delays and empirical mapping functions indicate large biases ranging between 18 and 90 mm, which are considered to be caused by a significant variability of water vapor. According to the position error simulation, highly variability of the errors is clearly associated with severe atmospheric phenomena. Such simulations are very useful to investigate the behavior of the positioning errors due to local atmospheric disturbances. Finally, we compared PPP processed position solution using KARAT with that using the latest mapping function for the two week GEONET data sets. The KARAT solution were almost identical to the solution using GMF with linear gradient model, but some cases were slightly worse under the extreme atmospheric condition. Though we need further investigations to evaluate the capability of KARAT to reduce atmospheric path delays under the various topographic and meteorological regimes, the KARAT will be the powerful tool to reduce atmospheric path delay with the numerical weather model improvement.

ACKNOWLEDGMENTS

We would like to thank the Geographical Survey Institute, Japan for providing GEONET data sets. We also thank the Japan Meteorological Agency for providing data and products.

REFERENCES

Bar-Sever, Y. E. and P. M. Kroger, Estimating horizontal gradients of tropospheric path delay with a single GPS receiver, J. Geophys. Res., 103, pp.5019-5035, 1998.

Bevis, M., S. Businger, S. Chiswell, T. A. Herring, R. A. Anthes, C. Rocken and R. H. Ware, GPS meteorology: mapping zenith wet delays onto precipitable water, J. Appl. Met., 33, pp. 379-386, 1994.

Boehm, J. and H. Schuh, Vienna Mapping Functions in VLBI analyses, Geophys. Res. Lett., 31, L01603, doi:10.1029/2003GL018984, 2004.

Boehm, J., A. Niell, P. Tregoning, and H. Schuh, Global Mapping Function (GMF): A new empirical mapping function based on numerical weather model data, Geophys. Res. Lett., 33, L07304, 2006a.

Boehm, J., B. Werl, and H. Schuh, Troposphere mapping functions for GPS and very long baseline interferometry from European Centre for Medium-Range Weather Forecasts operational analysis data, J. Geophys.Res., 111, B02406, 2006b.

Chen, G. and T. A. Herring, Effects of atmospheric azimuthal asymmetry on the analysis of space geodetic data, Geophys, Res. Lett., 102, 20489-20502, 1997.

Hobiger, T., R. Ichikawa, T. Takasu, Y. Koyama and T. Kondo, Ray-traced troposphere slant delays for precise point positioning, Earth Planets Space, 60, 5, e1-e4, 2008a.

Hobiger, T., R. Ichikawa, Y. Koyama and T. Kondo, Fast and accurate ray-tracing algorithms for real-time space geodetic applications using numerical weather models, Journal of Geophysical Research, under review, 2008b.

Hobiger, T., R. Ichikawa, Y. Koyama and T. Kondo, Kashima Ray-tracing Service (KARATS) –On-line provision of total troposphere slant delay corrections for East Asian sites, in this issue, 2008c.

MacMillan, D.S., Atmospheric gradients from very long baseline interferometry observations, Geophys. Res. Lett., 22, pp.1041-1044, 1995.

Niell, A. E., Global mapping functions for the atmosphere delay at radio wavelengths, J. Geophys. Res., 101(B2), 3227–3246, 1996.

Niell, A. E., Preliminary evaluation of atmospheric mapping functions based on numerical weather models, Phys. Chem. Earth, 26, 475–480, 2001.

Saito, K., et al., The Operational JMA Nonhydrostatic Mesoscale Model, Monthly Weather Review, 134, 1266-1298, 2006.

Saastamoinen, J., Contributions to the theory of atmospheric refraction, part 2, Bull. G'eod'esique, 107, 13-34, 1972.

Takasu, T. and S. Kasai, Evaluation of GPS Precise Point Positioning (PPP) Accuracy, IEIC Technical Report, 105(208), 40–45, 2005.